Bipolar optical force on a dipolar nanoparticle: Thermally induced switching between optical pulling and optical pushing

Jiangnan Ma,[1] Lv Feng,[1] Zijun Sun,[1] Xiangsuo Fan,[2] Lixin Ge,[3] Zhifang Lin,[4] Hongxia Zheng,[1,4,5,*] and Huajin Chen[1,4,5,6,†]

[1]*School of Electronic Engineering, Guangxi University of Science and Technology, Liuzhou, Guangxi 545006, China*
[2]*School of Automation, Guangxi University of Science and Technology, Liuzhou, Guangxi 545006, China*
[3]*School of Physics and Electronic Engineering, Xinyang Normal University, Xinyang 464000, China*
[4]*State Key Laboratory of Surface Physics and Department of Physics, Fudan University, Shanghai 200433, China*
[5]*Guangxi Key Laboratory of Multidimensional Information Fusion for Intelligent Vehicles, Liuzhou, Guangxi 545006, China*
[6]*Guangxi Earthmoving Machinery Collaborative Innovation Center, Liuzhou, Guangxi 545006, China*

(Received 7 June 2023; revised 2 September 2023; accepted 28 September 2023; published 13 October 2023)

The ability to readily switch between optical pulling and pushing forces on micro-objects is both important and fascinating for arbitrary optical manipulations. The bipolar optical force (namely, optical pulling versus optical pushing) on an object can be achieved generally by elaborately tailoring illuminating optical fields and/or surrounding media. Here, we propose an approach to achieve the temperature-reconfigured bipolar optical force on a dipolar nanoparticle. The basic idea is demonstrated on a particle immersed in a Bessel beam and made of material exhibiting a temperature-induced reversible transition, such as vanadium dioxide. Numerical results based on the decomposed force expressions indicate that the optical pulling force originates from the recoil force dominated by the coupling of electric and magnetic dipoles simultaneously excited on the particle, while the optical pushing force comes mostly from the interception force, which surpasses the recoil force when the excitation of the magnetic dipole is suppressed. Our dynamical simulations show that the nanoparticle can be transversely trapped stably in the vicinity of maximum light intensity while longitudinally switchable between the pulling against and pushing along light propagation. The bipolar characteristic does not require any change of the manipulating light or ambient material, opening interesting possibilities in flexible optical manipulations.

DOI: 10.1103/PhysRevB.108.134308

I. INTRODUCTION

When light shines on an object, it can exert an optical force and thus push the object along its propagating direction. Known as radiation pressure [1–3], such a force was first applied by Ashkin in 1970 to practical optical manipulations [4]. A decade ago, a counterintuitive phenomenon, i.e., optical pulling force [5–9], was discovered and has captured increasing interest, since it adds one significant manipulation freedom [10–13]. In contrast to a conventional optical pushing force, an optical pulling force can be thought of as a negative type of radiation pressure, which points in a direction opposite to the local wave momentum, or against the light propagation.

The discovery of an optical pulling force indeed suggests a bipolar characteristic of the optical force, provided that the optical pushing and optical pulling on the same object can be conveniently switched to and fro. The bipolar trait is expected to offer quite a few new functionalities and applications [14], adding considerably to the diversity of flexible optical manipulation. A variety of approaches have thus demonstrated the bipolar feature of the optical force. Up to now, such approaches fall into two categories, either by elaborately tailoring the illumination light field, or by intricately engineering the structured material background. The former category relies on structured light [15] by tailoring the property parameters of the constituent waves that form the illumination, such as polarizations [9,16], amplitudes and/or phases [8,17], propagating directions [18], and wavelength [19]. The latter employs hyperbolic metamaterials [20,21], plasmonic substrates [22], and photonic crystals [23] as the structured material background.

In this paper, we report an alternative method to realize the reconfigurable bipolar optical forces (i.e., optical pulling versus optical pushing) exerted on a dipolar nanoparticle, which is accomplished through tuning the temperature of the illuminated nanoparticle. As a proof-of-principle demonstration, we focus on a nanoparticle made of vanadium dioxide (VO_2), which is known for a reversible insulator-metal transition, occurring at a critical temperature T_c about 340 K [24,25]. During the solid-solid phase transition between the low-temperature insulating monoclinic phase and the high-temperature metallic rutile phase in a picosecond timescale [26], VO_2 exhibits an ultrafast dramatic change of optical properties as well as electrical conductivity. Such a feature brings about many intriguing applications in fields as varied as semiconductors [27] and metamaterials [28,29]. We here demonstrate the temperature-controlled bipolar optical force on a dipolar VO_2 particle illuminated by a Bessel

*hxzheng18@fudan.edu.cn
†huajinchen13@fudan.edu.cn

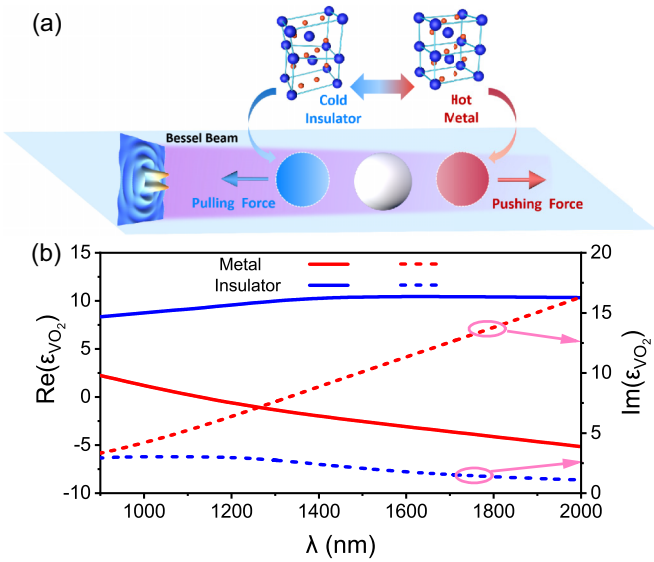

FIG. 1. (a) Schematic illustration of temperature-switched bipolar optical force on a VO_2 nanoparticle illuminated by a Bessel beam propagating rightwards. The optical force exerted on the particle switched from pushing (rightwards) to pulling (leftwards) when VO_2 undergoes a transition from metal to insulator. The two blue, three-dimensional frames represent the molecular structures of a VO_2 nanoparticle in the insulating monoclinic and metallic orthorhombic phases, respectively. (b) The dielectric permittivity diagram of VO_2 vs the wavelength in metallic (red lines) and insulating (blue lines) phases, respectively.

beam. For other phase-transition materials accompanied by a significant change of optical property, an approach for the inverse design of an optical field [30] can be employed to construct an optimized structured light field to implement the temperature-switched bipolar feature.

II. RESULTS AND DISCUSSION

The schematic of a temperature-switched bipolar optical force is illustrated in Fig. 1(a). Here, we consider a VO_2 nanoparticle immersed in water (with a fixed refractive index $n_{\text{ref}} = 1.33$ supposed) and illuminated by a Bessel beam. The VO_2 nanoparticle can be subject to a pulling or pushing force when it undergoes a transition between the insulating monoclinic ($T < T_c$) and metallic orthorhombic ($T > T_c$) phases. The electric field of the Bessel beam propagating along the z direction is given by [31]

$$\mathbf{E}(\mathbf{r}) = E_{\text{axis}} e^{ik_z z}\{\mathbf{e}_x[J_0(\sigma) + J_2(\sigma)P_\perp \cos 2\phi] + \mathbf{e}_y[J_2(\sigma)P_\perp \sin 2\phi] - \mathbf{e}_z[2\,\mathrm{i}J_1(\sigma)P_\parallel \cos\phi]\}, \quad (1)$$

where E_{axis}, dependent on the amplitude of the electric field E_0, is the on-axis electric field component of the Bessel beam, J_j denotes the Bessel function of order j, $\sigma = k\rho \sin\alpha_0$, $P_\perp = \frac{1-\cos\alpha_0}{1+\cos\alpha_0}$, $P_\parallel = \frac{\sin\alpha_0}{1+\cos\alpha_0}$, and $k_z = k\cos\alpha_0$, with k and α_0 being the wave number in the medium and cone angle of the Bessel beam. (ρ, ϕ, z) represent the cylindrical coordinates. The VO_2 nanoparticle can be synthesized via a template-free hydrothermal method [32], and its dielectric permittivity versus the wavelength is presented in Fig. 1(b), where solid and dashed lines represent the real and imaginary parts, respectively. The red and blue lines are corresponding to, respectively, the metallic phase and insulating phase, agreeing with the results of Refs. [33–35].

To illustrate the temperature-controlled bipolar optical force acting on a VO_2 nanoparticle, we compute the longitudinal optical force F_z based on the generalized Lorenz-Mie theory [36]. The explicit force expression reads [37–39]

$$F_z = -F_0 \,\mathrm{Re}\sum_{n=1}^{\infty}\sum_{m=-n}^{n}\left[c_{m,n}^{(1)} f_{m,n}^{(1)} + c_{m,n}^{(2)} f_{m,n}^{(2)}\right], \quad (2)$$

where $F_0 = 4\pi\varepsilon_b E_0^2/k^2$ with ε_b being the permittivity in the background. The indices n and m are both integers satisfying $n \geqslant 1$ while $-n \leqslant m \leqslant n$. In all our numerical calculations, n is truncated at $n_{\max} = 10$. The constant coefficients $c_{m,n}^{(1)}$ and $c_{m,n}^{(2)}$ are

$$c_{m,n}^{(1)} = \frac{m}{n(n+1)},$$
$$c_{m,n}^{(2)} = \left[\frac{n(n+2)(n-m+1)(n+m+1)}{(n+1)^2(2n+1)(2n+3)}\right]^{1/2}, \quad (3)$$

while $f_{m,n}^{(1)}$ and $f_{m,n}^{(2)}$ depend on the scatters and incident optical field by

$$f_{m,n}^{(1)} = a_{m,n}b_{m,n}^* - \frac{1}{2}(p_{m,n}b_{m,n}^* + a_{m,n}q_{m,n}^*),$$
$$f_{m,n}^{(2)} = a_{m,n}a_{m,n+1}^* + b_{m,n}b_{m,n+1}^* - \frac{1}{2}(a_{m,n}p_{m,n+1}^* + p_{m,n}a_{m,n+1}^* + b_{m,n}q_{m,n+1}^* + q_{m,n}b_{m,n+1}^*). \quad (4)$$

The superscript * denotes the complex conjugate. $(p_{m,n}, q_{m,n})$ and $(a_{m,n}, b_{m,n})$ are the expansion coefficients of the incident field (also termed the beam shape coefficients [36]) and the scattering field in terms of the vector spherical wave function (see, e.g., Ref. [37]), respectively.

Figure 2 shows the phase diagrams of the optical force F_z on the VO_2 sphere in the insulating and metallic phases as functions of the incident wavelength λ and the particle radius R. Here, as an example, the polar angle of the Bessel beam $\alpha_0 = 87^\circ$, and the field amplitude $E_0 = 8.68 \times 10^6$ V/m with its intensity at the beam axis being 100 mW/μm^2. Under illumination of such a beam, the temperature increase originating from the particle absorption-induced heating effect is evaluated to be about a few Kelvin by using the method proposed in Refs. [40–42], bringing it well below the critical temperature. The particle can therefore well remain in an insulating phase at low temperatures until the phase transition method is utilized. For the insulating phase [Fig. 2(a)], the colored and white regions denote the pulling ($F_z < 0$) and pushing ($F_z > 0$) forces. For the metallic phase [Fig. 2(b)], however, F_z is always positive, indicating that the particle is always subject to a pushing force. As a result, the bipolar optical force is implemented in the color area in Fig. 2(a). For the parameter space given in Fig. 2, the bipolar force will totally vanish when $\alpha_0 < 77^\circ$.

To trace the physical origin of the bipolar optical force, we decompose the longitudinal force into the interception ${}^I F_z$ and recoil ${}^R F_z$ parts [6,39],

$$F_z = {}^I F_z + {}^R F_z, \quad (5)$$

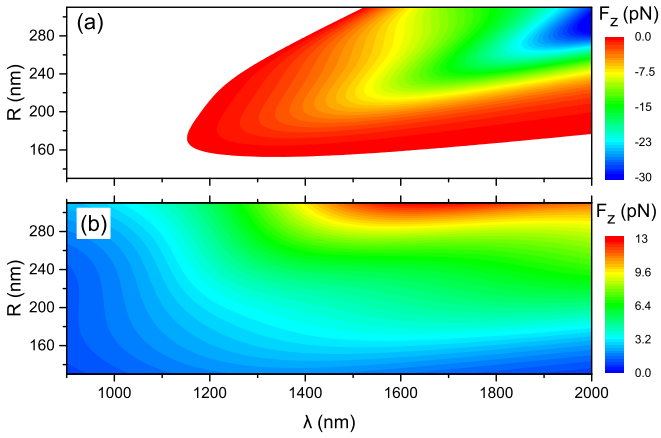

FIG. 2. Phase diagrams of longitudinal optical force F_z on a VO_2 particle vs the incident wavelength λ and the particle radius R in the cases where the particle is in (a) the insulating phase and (b) the metallic phase. The $F_z < 0$ and $F_z > 0$ denote the optical pulling and pushing forces, respectively. The color area in (a) indicates that the particle is exerted by a pulling force in the insulator phase while it is subject to a pushing force if in the metallic phase, as visualized in (b).

with

$$
\begin{aligned}
{}^{I}F_z = \frac{F_0}{2}\,\mathrm{Re}\sum_{n=1}^{\infty}\sum_{m=-n}^{n} & c_{m,n}^{(1)}(p_{m,n}b_{m,n}^{*} + a_{m,n}q_{m,n}^{*}) \\
& + c_{m,n}^{(2)}(a_{m,n}p_{m,n+1}^{*} + p_{m,n}a_{m,n+1}^{*} \\
& + b_{m,n}q_{m,n+1}^{*} + q_{m,n}b_{m,n+1}^{*}), \\
{}^{R}F_z = -F_0\,\mathrm{Re}\sum_{n=1}^{\infty}\sum_{m=-n}^{n} & c_{m,n}^{(1)}(a_{m,n}b_{m,n}^{*}) \\
& + c_{m,n}^{(2)}(a_{m,n}a_{m,n+1}^{*} + b_{m,n}b_{m,n+1}^{*}).
\end{aligned}
\tag{6}
$$

The interception force ${}^{I}F_z$ arises from the coupling between the multipoles excited in the particles and the incident field, while the recoil force ${}^{R}F_z$ stems from the interaction between various multipoles excited in the particles. In Fig. 3 we display ${}^{I}F_z$ (orange dotted-dashed line) and ${}^{R}F_z$ (pink dashed line) versus the incident wavelength λ for the cases where the particle is in the insulating and metallic phases, taking a particle radius $R = 180$ nm as an example. For both phases, the interception force ${}^{I}F_z$ always points in the direction of light propagation (with ${}^{I}F_z > 0$). For the insulator phase, the recoil force ${}^{R}F_z$ is negative and its magnitude surpasses the positive interception force, leading to optical pulling when $\lambda > 1150$ nm. For the metallic phase, however, although the recoil force is negative in the range roughly from 900 to 1840 nm, it is much smaller in magnitude compared with the interception force, leaving us with a positive F_z, as illustrated in Fig. 3(b).

To gain further insight, we partition ${}^{R}F_z$ into contributions from the couplings between various multipoles. Figures 3(c) and 3(d) show the partitioned forces for the insulating and metallic phases, respectively. They are F_{pm}, which comes from the interaction between electric and magnetic dipoles, and $F_{Q^e p}$ ($F_{Q^m m}$) which arises from the coupling between an electric (magnetic) dipole and electric (magnetic) quadrupole.

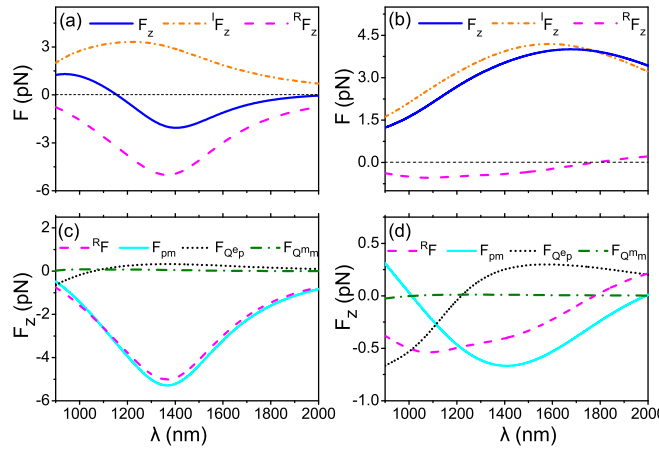

FIG. 3. Longitudinal optical force F_z and its interception ${}^{I}F_z$ and recoil ${}^{R}F_z$ parts exerted on a VO_2 nanoparticle of $R = 180$ nm in the (a) insulating and (b) metallic phases. (c) and (d) The decomposed optical forces in Eq. (7) that contribute significantly to the recoil force ${}^{R}F_z$ corresponding to (a) and (b), respectively. All other parameters are the same as those in Fig. 2.

The partitioned forces are given explicitly by

$$
\begin{aligned}
F_{pm} &= -F_0\,\mathrm{Re}\sum_{m=-1}^{1} c_{m,1}^{(1)}(a_{m,1}b_{m,1}^{*}), \\
F_{Q^e p} &= -F_0\,\mathrm{Re}\sum_{m=-1}^{1} c_{m,1}^{(2)}(a_{m,1}a_{m,2}^{*}), \\
F_{Q^m m} &= -F_0\,\mathrm{Re}\sum_{m=-1}^{1} c_{m,1}^{(2)}(b_{m,1}b_{m,2}^{*}).
\end{aligned}
\tag{7}
$$

In both phases the negative recoil forces originate mainly from the coupling between the multipoles of lowest order, namely, between the electric and magnetic dipoles, as manifested by F_{pm} displayed by the cyan lines in Figs. 3(c) and 3(d). For the insulating phase, while the electric and magnetic dipoles are simultaneously excited, multipoles of higher orders are rather weak, resulting in an overwhelming and negative F_{pm} that brings about a pulling force in a certain range of manipulating wavelengths. For the metallic phase, nevertheless, the excitation of the magnetic dipole is substantially suppressed, leading to a much smaller F_{pm} that fails to predominate over the positive interception force and thus leaving us with a pushing force. The temperature-induced switching between the insulating and metallic phases stimulates and restrains the excitation of the magnetic dipole, featuring the bipolarity of the longitudinal force on a dipolar nanoparticle, without resorting to the change of the manipulating light or the surrounding material. It is noted that core-shell structures are usually employed to simultaneously excite electric and magnetic dipoles for implementing optical pulling on nanoparticles [43,44]. In our case a homogeneous insulator (dielectric) particle is found to support a pulling force with the same physical mechanism.

A negative longitudinal force F_z does not necessarily mean stable optical pulling, unless it is in the coincident presence of transverse trapping that confines the particle in the

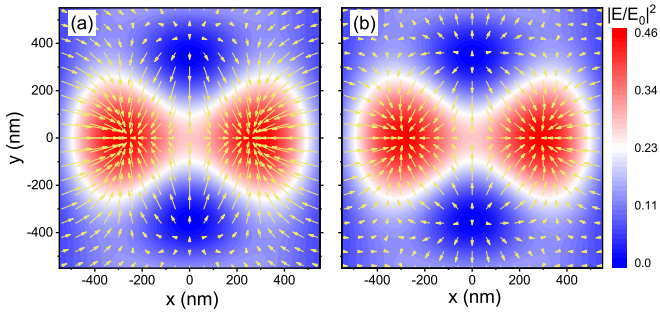

FIG. 4. Transverse optical forces vs the particle position in the transverse *xoy* plane for the (a) insulating and (b) metallic phases. The yellow arrows denote the magnitude and direction of the transverse forces. The intensity profiles are also presented as the background. All other parameters are the same as those in Fig. 3 except that the illuminating wavelength is specified as $\lambda = 1550$ nm.

pulling area. To corroborate the stability, we compute the transverse optical forces on the VO_2 nanoparticle for both insulating and metallic phases. The results are displayed in Figs. 4(a) and 4(b), where the arrows denote the magnitude and direction of the transverse forces. Superimposed on the graph are the intensity profiles of the electric field. The illuminating wavelength is $\lambda = 1550$ nm as an example for demonstration. Stable transverse trapping in the proximity of intensity maxima $(x, y) = (\pm 250, 0)$ nm is visualized for both phases, implying that the nanoparticle is stably subject to either optical pulling or optical pushing, exhibiting an intriguing bipolar feature induced exclusively by temperature, or, equivalently, triggered solely by an ultrafast photoexcitation [26].

The dynamical simulations of the particle trajectories in Fig. 5 provide a direct visualization of particle motion in

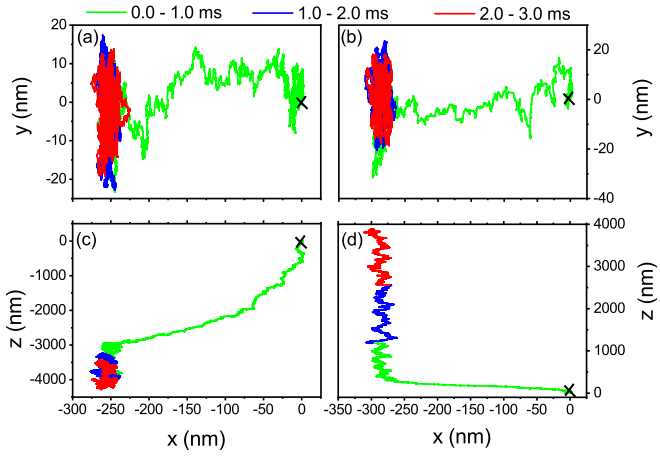

FIG. 5. Dynamical simulation of the particle trajectories for the (a), (c) insulating and (b), (d) metallic phases. The transverse and longitudinal motions of the particle are displayed in (a), (b) and (c), (d), respectively. The black crosses at the coordinate origin denote the initial positions of the particle, and the three colors, green, blue, and red, indicate three different periods of time. All other parameters are the same as those in Fig. 4.

our situation. The processes are described by the Langevin equation [45,46] $m\frac{d^2\mathbf{x}}{d^2t} = \mathbf{F}(x,t) - \gamma\frac{d\mathbf{x}}{dt} + \mathbf{R}$. Here, $\mathbf{x}$ is the center position of the particle on the beam plane, $\mathbf{F}(x,t)$ is the corresponding in-plane optical force acting on the particle with mass $m = \rho V$, the ρ denotes the density, and V is the volume of the particle. The damping coefficient γ is given by $\gamma = 6\pi\eta r_s$ for a particle with radius r_s, where $\eta = 0.89 \times 10^{-3}$ Pa s is the viscosity of the water. When performing the calculation at each time interval h, a new value of the stochastic Brownian force $\mathbf{R}$ during the new interval should be drawn from a Gaussian random generator with standard deviation $\sigma = \sqrt{2\gamma k_B T/h}$, where k_B is Boltzmann's constant and T is the temperature of water.

The dynamical simulations for the insulating and metallic phases are presented in Figs. 5(a), 5(c) and Figs. 5(b), 5(d). The transverse (longitudinal) motions of the particle are displayed in Figs. 5(a) and 5(b) [Figs. 5(c) and 5(d)]. In either phase, the particle, initially located at the coordinate origin $(x, y) = (0, 0)$, is driven by the transverse optical force to near $(x, y) = (-250, 0)$ nm, where it is trapped in the vicinity of maximum light intensity, as visualized in Figs. 5(a) and 5(b). Meanwhile, the particle is pulled against the light propagation (in the $-z$ direction) if it is in the insulating phase, as shown in Fig. 5(c), while it is pushed along the light propagation (in the $+z$ direction) if it is in the metallic phase, as shown in Fig. 5(d). The dynamical behavior of the particle corroborates the bipolarity in the longitudinal optical force with respect to pulling and pushing, which can be triggered by a temperature change, or, equivalently, through an ultrafast laser pulse in a timescale of several picoseconds.

III. CONCLUSION

In summary, we have presented an in-principle demonstration of the temperature-switched bipolar optical forces (optical pulling and pushing forces) with a dipolar particle made of VO_2 material under the illumination of a Bessel beam. The bipolarity is attributed to the ultrafast reversible temperature-induced (or photoinduced) transition between the insulator and metal phases of the optically manipulated particle. In either phase, the interception part ${}^{I}F_z$ of the longitudinal optical force F_z is pushing, with ${}^{I}F_z > 0$. While the recoil part ${}^{R}F_z$ of F_z may be negative, only in the insulating phase can it predominate over the ${}^{I}F_z$, giving rise to an optical pulling force $F_z < 0$. The underlying physics lies in that under the illumination of the Bessel beam, both the electric and magnetic dipoles are efficiently excited on the nanoparticle in the insulating phase, bringing about a substantial enhancement of the dipole coupling that makes the surpassing pulling contribution. In the metallic phase, on the other hand, the excitation of the magnetic dipole is substantially suppressed, resulting in conventional optical pushing. In addition, the particle is transversely trapped, regardless of its phase, in the proximity of maximum light intensity where optical pulling and pushing occur for different phases, facilitating optical manipulation. Finally, our dynamical simulation of the particle motion further substantiates the bipolarity that can be switched by temperature, or, equivalently, triggered by ultrafast photoexcitation as well as the absorption-induced

heating through tuning the beam intensity in practice. The temperature-controlled bipolar effect of optical pulling and pushing provides an additional degree of freedom for optical manipulations. Although the bipolar force cannot be realized with general Bessel beams of arbitrary order, it is expected to be universal for many other phase-changing materials [47] through designing structured light fields with the recently proposed inverse design approach [30].

ACKNOWLEDGMENT

This work was supported by National Natural Science Foundation of China (12174076, 12204117, and 12074084), Guangxi Science and Technology Project (2021GXNSFDA196001, 2023GXNSFFA026002, 2022AC21108, AD22080042, and AB21220052), and Open Project of State Key Laboratory of Surface Physics in Fudan University (KF2022_15).

[1] J. C. Maxwell, *A Treatise on Electricity and Magnetism* (Clarendon Press, Oxford, UK, 1873).
[2] P. Lebedew, Ann. Phys. (Berlin) **311**, 433 (1901).
[3] E. F. Nichols and G. F. Hull, Phys. Rev. (Series I) **13**, 307 (1901).
[4] A. Ashkin, Phys. Rev. Lett. **24**, 156 (1970).
[5] S.-H. Lee, Y. Roichman, and D. G. Grier, Opt. Express **18**, 6988 (2010).
[6] J. Chen, J. Ng, Z. Lin, and C. T. Chan, Nat. Photonics **5**, 531 (2011).
[7] A. Novitsky, C.-W. Qiu, and H. Wang, Phys. Rev. Lett. **107**, 203601 (2011).
[8] S. Sukhov and A. Dogariu, Phys. Rev. Lett. **107**, 203602 (2011).
[9] O. Brzobohatý, V. Karásek, M. Šiler, L. Chvátal, T. Čižmár, and P. Zemánek, Nat. Photonics **7**, 123 (2013).
[10] A. Dogariu, S. Sukhov, and J. Sáenz, Nat. Photonics **7**, 24 (2013).
[11] W. Ding, T. Zhu, L.-M. Zhou, and C.-W. Qiu, Adv. Photonics **1**, 024001 (2019).
[12] H. Li, Y. Cao, L.-M. Zhou, X. Xu, T. Zhu, Y. Shi, C.-W. Qiu, and W. Ding, Adv. Opt. Photonics **12**, 288 (2020).
[13] Y. Shi, Q. Song, I. Toftul, T. Zhu, Y. Yu, W. Zhu, D. P. Tsai, Y. Kivshar, and A. Q. Liu, Appl. Phys. Rev. **9**, 031303 (2022).
[14] E. Lee, D. Huang, and T. Luo, Nat. Commun. **11**, 2404 (2020).
[15] A. Forbes, M. de Oliveira, and D. M. R, Nat. Photonics **15**, 253 (2021).
[16] V. Shvedov, A. R. Davoyan, C. Hnatovsky, N. Engheta, and W. Krolikowski, Nat. Photonics **8**, 846 (2014).
[17] D. B. Ruffner and D. G. Grier, Phys. Rev. Lett. **109**, 163903 (2012).
[18] R. Ali, R. Dutra, F. Pinheiro, and P. M. Neto, Opt. Lett. **46**, 1640 (2021).
[19] L.-F. Yang and K. J. Webb, Phys. Rev. B **103**, 245124 (2021).
[20] R. Jin, Y. Xu, Z.-G. Dong, and Y. Liu, Nano Lett. **21**, 10431 (2021).
[21] A. Ivinskaya, N. Kostina, A. Proskurin, M. I. Petrov, A. A. Bogdanov, S. Sukhov, A. V. Krasavin, A. Karabchevsky, A. S. Shalin, and P. Ginzburg, ACS Photonics **5**, 4371 (2018).
[22] M. I. Petrov, S. V. Sukhov, A. A. Bogdanov, A. S. Shalin, and A. Dogariu, Laser Photonics Rev. **10**, 116 (2016).
[23] N. Kostina, M. Petrov, V. Bobrovs, and A. S. Shalin, Opt. Lett. **47**, 4592 (2022).
[24] F. J. Morin, Phys. Rev. Lett. **3**, 34 (1959).
[25] A. Zylbersztejn and N. F. Mott, Phys. Rev. B **11**, 4383 (1975).
[26] A. Cavalleri, C. Tóth, C. W. Siders, J. A. Squier, F. Ráksi, P. Forget, and J. C. Kieffer, Phys. Rev. Lett. **87**, 237401 (2001).
[27] M. Wuttig, H. Bhaskaran, and T. Taubner, Nat. Photonics **11**, 465 (2017).
[28] L. Lei, F. Lou, K. Tao, H. Huang, X. Cheng, and P. Xu, Photonics Res. **7**, 734 (2019).
[29] T. Kang, B. Fan, J. Qin, W. Yang, S. Xia, Z. Peng, B. Liu, S. Peng, X. Liang, T. Tang, L. Deng, Y. Luo, H. Wang, Q. Zhou, and L. Bi, Photonics Res. **10**, 373 (2022).
[30] X. Zhao, H. Lin, H. Chen, H. Zheng, and J. Ng, Nanophotonics **12**, 2019 (2023).
[31] T. Čižmár, V. Kollárová, Z. Bouchal, and P. Zemánek, New J. Phys. **8**, 43 (2006).
[32] K. Liu, S. Lee, S. Yang, O. Delaire, and J. Wu, Mater. Today **21**, 875 (2018).
[33] I. Pirozhenko and A. Lambrecht, Phys. Rev. A **77**, 013811 (2008).
[34] R. Castillo-Garza, C.-C. Chang, D. Jimenez, G. L. Klimchitskaya, V. M. Mostepanenko, and U. Mohideen, Phys. Rev. A **75**, 062114 (2007).
[35] L. Ge, X. Shi, Z. Xu, and K. Gong, Phys. Rev. B **101**, 104107 (2020).
[36] G. Gouesbet, Opt. Commun. **283**, 517 (2010).
[37] J. Ng, Z. F. Lin, C. T. Chan, and P. Sheng, Phys. Rev. B **72**, 085130 (2005).
[38] N. Wang, J. Chen, S. Liu, and Z. Lin, Phys. Rev. A **87**, 063812 (2013).
[39] H. Chen, Q. Ye, Y. Zhang, L. Shi, S. Liu, Z. Jian, and Z. Lin, Phys. Rev. A **96**, 023809 (2017).
[40] Y. Zhou, X. Xu, Y. Zhang, M. Li, S. Yan, M. Nieto-Vesperinas, B. Li, C.-W. Qiu, and B. Yao, Proc. Natl. Acad. Sci. USA **119**, e2209721119 (2022).
[41] J. Lu, H. Yang, L. Zhou, Y. Yang, S. Luo, Q. Li, and M. Qiu, Phys. Rev. Lett. **118**, 043601 (2017).
[42] X. Xu, C. Cheng, H. Xin, H. Lei, and B. Li, Sci. Rep. **4**, 3989 (2014).
[43] N. Wang, W. Lu, J. Ng, and Z. Lin, Opt. Lett. **39**, 2399 (2014).
[44] H. Chen, S. Liu, J. Zi, and Z. Lin, ACS Nano **9**, 1926 (2015).
[45] X. Xu, Y. Yang, L. Chen, X. Chen, T. Wu, Y. Li, X. Liu, Y. Zhang, and B. Li, Laser Photonics Rev. **15**, 2000546 (2021).
[46] X. Xu, M. Nieto-Vesperinas, C.-W. Qiu, X. Liu, D. Gao, Y. Zhang, and B. Li, Laser Photonics Rev. **14**, 1900265 (2020).
[47] Y. Chen, X. Li, X. Luo, S. A. Maier, and M. Hong, Photonics Res. **3**, 54 (2015).